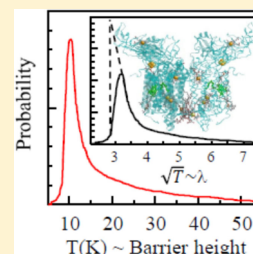# Conformational Changes in Pigment–Protein Complexes at Low Temperatures—Spectral Memory and a Possibility of Cooperative Effects

Mehdi Najafi,[†] Nicoleta Herascu,[†] Golia Shafiei,[†] Rafael Picorel,[‡] and Valter Zazubovich*[,†]

[†]Department of Physics, Concordia University, 7141 Sherbrooke Street West, Montreal, Quebec H4B 1R6, Canada
[‡]Estacion Experimental de Aula Dei (CSIC), Avda. Montañana 1005, 50059 Zaragoza, Spain

ABSTRACT: We employed nonphotochemical hole burning (NPHB) and fluorescence line narrowing (FLN) spectroscopies to explore protein energy landscapes and energy transfer processes in dimeric Cytochrome b_6f, containing one chlorophyll molecule per protein monomer. The parameters of the energy landscape barrier distributions quantitatively agree with those reported for other pigment–protein complexes involved in photosynthesis. Qualitatively, the distributions of barriers between protein substates involved in the light-induced conformational changes (i.e., −NPHB) are close to glass-like $\sim 1/\sqrt{V}$ (V is the barrier height) and not to Gaussian. There is a high degree of correlation between the heights of the barriers in the ground and excited states in individual pigment–protein systems, as well as nearly perfect spectral memory. Both NPHB and hole recovery are due to phonon-assisted tunneling associated with the increase of the energy of a scattered phonon. As the latter is unlikely for simultaneously both the hole burning and the hole recovery, proteins must exhibit a NPHB mechanism involving diffusion of the free volume toward the pigment. Entities involved in the light-induced conformational changes are characterized by md^2 value of about 1.0×10^{-46} kg·m². Thus, these entities are protons or, alternatively, small groups of atoms experiencing sub-Å shifts. However, explaining all spectral hole burning and recovery data simultaneously, employing just one barrier distribution, requires a drastic decrease in the attempt frequency to about 100 MHz. This decrease may occur due to cooperative effects. Evidence is presented for excitation energy transfer between the chlorophyll molecules of the adjacent monomers. The magnitude of the dipole–dipole coupling deduced from the Δ-FLN spectra is in good agreement with the structural data, indicating that the explored protein was intact.

1. INTRODUCTION

Understanding protein energy landscapes in photosynthetic pigment–protein complexes is important both from the general life sciences perspective (information on hierarchal protein energy landscapes[1–3] is necessary to better understand protein conformational changes and folding; see the famous Levinthal's paradox, for example) and in photosynthesis research per se (protein dynamics is affecting optical properties, energy, and charge transfer processes in proteins involved in photosynthesis). In optical experiments the dynamics of amorphous solids, including proteins, manifests as light- and thermally induced shifts of spectral lines of the pigments embedded in the solid. These shifts are directly observable in the single molecule/single photosynthetic complex spectroscopy (SPCS) experiments.[3,4] In the ensemble spectra these shifts manifest as spectral hole burning (SHB) and as hole recovery and broadening.[5] Collectively these phenomena are known as spectral diffusion. SHB involves selecting a subensemble of pigment molecules with zero-phonon lines (ZPL) in resonance with the laser and causing either the photochemical transformation of the molecules themselves or the rearrangement of their environment. In amorphous solids, including proteins at low temperatures, the light-induced rearrangement of the environment is the dominant process. On the ensemble level this mechanism is known as Nonphotochemical Hole Burning, NPHB.[6] In the case of SPCS these are just the light-induced

shifts of the spectral lines (as opposed to their disappearance). As the pigment molecule is not modified, the reverse conformational change gives rise to the recovery of a spectral hole or to spectral line returning to its original wavelength. Following NPHB, hole recovery and hole broadening offers one a window onto the distributions of barriers on the protein energy landscape.

The key aspects of the origins of light- and thermally induced shifts of the spectral lines, the basis of the observations in both SPCS and NPHB experiments, are demonstrated in Figure 1. Two hierarchal tiers of the protein energy landscape[3,4] are shown. For clarity, only two wells are shown for the higher, hierarchy-wise, tier of the energy landscape. Transitions between these two states correspond to NPHB and to the larger ones (several cm^{-1} or more) among the spectral shifts in the SPCS experiments.[3] Transitions between the wells of the lower tier of the energy landscape (fine structures are the bottoms of the deep wells) contribute mostly to the width of the spectral hole or spectral line.[5] Before being resonantly excited with a photon with energy ΔE_1, the pigment–protein system is assumed to be in state 1. As the barriers in the excited electronic state (red) are lower than in the ground state (blue),
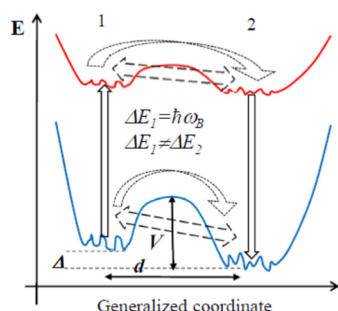
Figure 1. Energy landscapes of a pigment−protein system in ground (blue) and excited (red) electronic states. Two tiers of the protein energy landscape are shown. Vertical arrows indicate electronic transitions of the pigment, dashed straight arrows indicate tunneling, and curved dotted arrows indicate barrier hopping. Also shown are barrier height V, asymmetry Δ, and shift d (associated with the conformational change) along the generalized coordinate.

the system is more likely to experience a conformational change while the pigment is in the excited state and end up in state 2, characterized by different transition energy ΔE_2. The $1 \rightarrow 2$ transition may occur by virtue of either tunneling or barrier-hopping. Both tunneling and barrier-hopping are possible also in the ground state, albeit at much lower rates due to higher barriers. Transitions from state 2 to state 1 in the ground state contribute to the recovery of the spectral hole or to the return of the single-molecule line to its original transition frequency.

Photosynthetic pigment−protein complexes are particularly suitable as model systems for research on protein energy landscapes and dynamics utilizing optical methods. Chromophores are present in these complexes naturally, without extraneous manipulations, and in a wide variety of local environments. Recently we published several papers where NPHB was employed to study the energy landscapes in light-harvesting antenna complexes.[7−9] In particular, for the CP43 antenna complex we demonstrated that the distributions of barriers on the protein energy landscape are Gaussian and not proportional to $1/\sqrt{V}$[9] (V is the barrier height). The $\sim 1/\sqrt{V}$ distributions were predicted and observed in glasses;[10−12] a superposition of $1/\sqrt{V}$ and Gaussian terms was observed for phycobilisomes.[12] We also developed the novel unified approach to joint analysis and modeling of both hole burning and hole recovery data, for fixed temperature and upon temperature variations. Importantly, the logic used in ref 9 to arrive at the conclusion about the Gaussian shape of the barrier distributions in CP43 was independent of any features specific to proteins and distinguishing them from other amorphous solids, e.g., organic glasses. This logic relied on the fact that in the presence of "spectral memory" the barrier distributions encoded into the nonsaturated spectral holes and manifesting during the hole recovery (the "partial barrier distributions") differ from the full true barrier distributions (i.e., the distributions of all possible barriers on the relevant tier of the energy landscape, whether they are crossed in optical experiments or not). "Spectral memory" implies that spectral holes are recovered by the systems that had experienced NPHB returning to their preburn frequencies and not by the systems that were out of resonance with the laser in the beginning of the experiment and then evolved into resonance. In terms of Figure 1, the $1 \rightarrow 2 + 2 \rightarrow 1$ process dominates over $1 \rightarrow 2 + 2' \rightarrow 1'$ with accidental $\Delta E_1' = \Delta E_1$, the prime referring to another pigment−protein system. The partial barrier distribu-

tions are vastly different for different shapes of the true full distributions, and one can easily distinguish their manifestations. In the light of these CP43 results[9] it was tempting to suggest that the earlier results on hole recovery in glasses[10−12] could be misinterpreted, due to ignoring spectral memory as well as the spontaneous recovery at burn temperature, and ascribing all recovery to barrier hopping. If anything, organic glasses are more likely to have the pigment molecule in interaction with just one two-level system (TLS; the special low-temperature properties of amorphous solids are ascribed to the presence of TLS[13,14]) and to feature more perfect spectral memory than proteins with their multiwell energy landscapes. If true, this misinterpretation hypothesis would have far-reaching implications for the theories of amorphous solids at low temperatures[13,14] yielding the $\sim 1/\sqrt{V}$ barrier distributions. However, such a bold proposal obviously needed verification for other proteins and amorphous solids.

Additionally, even though we performed the experiments described in ref 9 on the red edge of the lowest-energy band of the CP43 complex in order to avoid any excitation energy transfer (EET)-related effects, CP43 is still a system of multiple relatively strongly coupled pigments.[15,16] Thus, although EET from the lowest-energy pigment or delocalized state was forbidden, we could not be completely confident that our results are free of the excitonic effects. For instance, if the lowest-energy excited state is partially delocalized over several interacting pigments, any of these pigments may experience a spectral shift triggered by optical excitation of this delocalized state. As different pigments of the CP43 complex are placed in somewhat different local environments, one cannot be fully sure that observed protein energy landscape parameters describe one particular pigment pocket of the protein.

Cytochrome (Cyt) $b_6 f$,[17−20] a complex containing just one chlorophyll a (Chl a) molecule per protein monomer, see Figure 2, represents a better model for protein energy
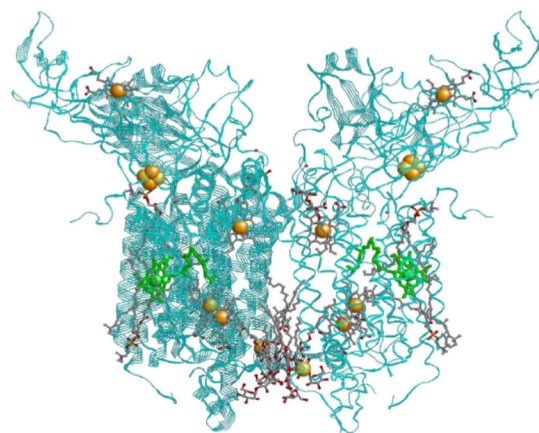

Figure 2. Structure of the Cyt $b_6 f$ dimer. PDB ID: 2E74.[17] Chlorophyll a molecules are highlighted in green. Iron atoms of hemes and iron−sulfur clusters are highlighted in gold. Cyan: protein. Orientation factor is 0.92 and the Mg−Mg distance is 6.1 nm.

landscapes research. It does not possess delocalized Chl a states and offers access to as uncontaminated optical manifestations of protein dynamics as possible. Cytochrome $b_6 f$, existing in vivo in dimeric form, mediates the transfer of electrons between the two photosynthetic reaction center complexes, Photosystem II and Photosystem I, while also

transferring protons across the thylakoid membrane from stroma to lumen. Most of the cofactors in Cyt b_6f are involved in these charge transfer processes and absorb at different wavelengths with respect to the Chl a. The exact purpose of that Chl a in Cyt b_6f is unclear.[18−20] Cytochrome b_6f was explored by both frequency- and time-domain spectroscopies.[18−20] It was shown that at least at room temperature the Chl a in Cyt b_6f exhibits unusually short fluorescence lifetime (∼250 ps) and reduced fluorescence yield, which were attributed to effective quenching of the Chl excitations by the aromatic groups of the protein. This quenching is considered the most likely reason why the presence of Chl a, although apparently useless from photosynthesis perspective and potentially dangerous (triplets), does not introduce any evolutionary disadvantage, and why Chl a remains preserved. Chlorophylls in Cyt b_6f are well screened by protein from the outside environment. The Mg-to-Mg distance between the two Chl molecules of the dimer is 6.1 nm, rendering the interaction between those Chl's very weak (dipole−dipole coupling $J_{12} \leq$ 0.4 cm^{-1}, depending on the dielectric constant). Below we are going to present the evidence of the slow excitation energy transfer between these two Chl's. The main focus of this manuscript, however, is on the protein energy landscapes. We employ the unified approach of ref 9 and determine the shape and quantitative parameters of the barrier distributions, as well as the likely nature of the entities involved in conformational changes. Taking this approach one step further and determining one single barrier distribution manifesting in SHB, the fixed-temperature hole recovery and the recovery upon thermocycling is possible if one invokes cooperative effects.

2. MATERIALS AND METHODS

Chloroplastic Cyt b_6f was isolated from market spinach according to Romanowska.[21] Two closely moving yellow bands were clearly observed around the middle of the sucrose gradient tubes, but both bands showed similar absorption spectra with the same heme/Chl a ratio. The stoichiometry resulted in approximately one Chl a per Cyt b_6f monomer using an extinction coefficient of 20 mM^{-1}·cm^{-1} for Cyt b as described in ref 21 and 75 mM^{-1}·cm^{-1} for Chl a as described in Pierre et al.[22] after sample reduction with sodium dithionite. For some experiments, the detergent n-octyl-β-D-glucopyranoside (OG) was replaced with n-dodecyl-β-D-maltoside (DM) in the final preparation by several dilution/concentration steps with 30 mM Tris/succinate, pH 6.5, and 0.03% (w/v) DM solution by centrifugation in 30 kDa MWCO Amicon tubes.

Absorption and broad spectral range hole spectra were measured with a Cary 5000 spectrophotometer with resolution of 0.1 nm. Broadband and selectively excited emission spectra and Δ-FLN (the difference of fluorescence line narrowed spectra before and after spectral hole burning) spectra were measured using Acton 2356 spectrograph with Princeton Instruments Pixis 1340 × 100 back-illuminated CCD. High-resolution spectra were measured with Sirah Matisse-DS frequency-stabilized tunable dye laser (bandwidth < 1 MHz). A 6 W 532 nm Spectra Physics Millennia was used as a pump laser. The sample was placed inside a liquid-helium bath/flow cryostat (Ukrainian Academy of Sciences).[23] High-resolution experiments were performed in fluorescence excitation mode, with vertically polarized excitation light and fluorescence collected at 90° with respect to the excitation and detected with a Hamamatsu photomultiplier/photon counting module.

The intensity of excitation light was stabilized by BEOC laser power controller and regulated with neutral density filters. The irradiance was ∼17 μW/cm^2 for burning; 500 times smaller irradiance was used for reading hole spectra. Thermocycling involves producing a spectral hole at low temperature (e.g., 5 K), temporarily increasing the temperature to a higher value, measuring the hole spectrum again at burn temperature, and then repeating the cycle with ever increasing maximal temperature. More details can be found in refs 8 and 9.

3. RESULTS

3.1. Absorption and Emission Spectra. Figure 3 depicts absorption (black), nonselectively excited emission (red), and
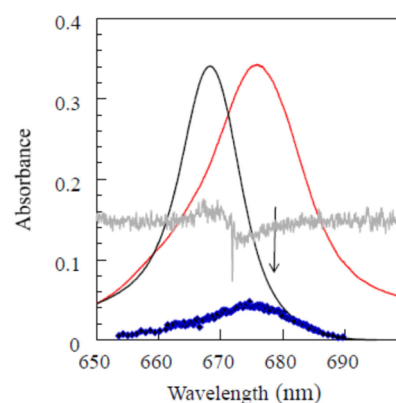

Figure 3. Absorption (black), emission excited at 600 nm (red), and SHB action (blue diamonds) spectra for Cyt b_6f at 5 K. Also presented is an example of a low-resolution hole in the absorption spectrum (gray). Arrow indicates the burn wavelength for HGK and recovery experiments described below.

hole burning (HB) action spectra (dark blue diamonds) of Cyt b_6f at 5 K. Also presented is an example of the low-resolution hole spectrum (gray). The latter demonstrates the shapes of the NPHB antihole and the pseudophonon sidehole. The zero-phonon hole is clearly visible, despite relatively poor resolution, suggesting that electron−phonon coupling is moderate. The emission spectrum was measured using excitation with white light through a band-pass interference filter centered at 600 nm and with the bandwidth of 10 nm to ensure selective excitation of Chl a. The HB action spectrum is the dependence of the hole depth on wavelength for fixed illumination dose; it was measured in fluorescence excitation mode. In the simplest possible scenario (no heterogeneity, no EET) it represents the site distribution function (SDF) of all pigments. In this case absorption and emission spectra would be shifted by the same amount to the blue and to the red of the action spectrum, respectively, and would be of similar width. It is clear that for Cyt b_6f this simple scenario is invalid. The sub-SDF of the most easily burnable pigments, represented by the action spectrum peaked at 674.6 nm and with the width of 16.6 nm, matches the emission spectrum peaked at 675.9 nm. The absorption spectrum, however, is peaked at 668.3 nm. Our emission and absorption spectra are both peaked ∼2.2 nm to the blue with respect to those reported in ref 18. The widths are fairly similar, 12.5 nm vs 11.6[18] for absorption spectra and 19 nm (16 nm[18]) for emission spectra. Note that in ref 18 as well the emission spectrum was significantly broader than the absorption spectrum. The systematic difference in spectral peak positions can be attributed to samples belonging to different organisms

(spinach here and *Synechocystis* PCC6803 in ref 18), to differences in isolation procedures (different detergents), as well as to Cyt b$_6$f in ref 18 being monomeric. (We confirmed that samples with dodecyl maltoside instead of the octyl glucopyranoside (see Materials and Methods) had both absorption and emission spectra red-shifted by about 1 nm.)

3.2. Energy Transfer and Δ-FLN Spectra. The emission spectrum is in agreement with the HB action spectrum, given the parameters of the single-site spectrum and electron−phonon coupling derived from the data in Figure 4. The latter
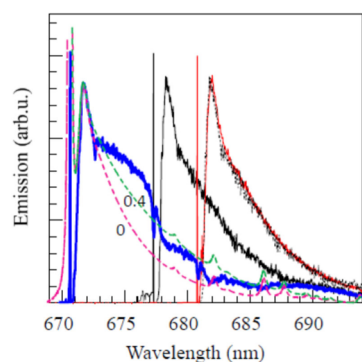

Figure 4. Noisy curves: Δ-FLN spectra obtained at 5 K with excitation at 670.7 (blue), 677.0 (black), and 680.8 (red) nm. The blue curve was measured after performing Δ-FLN experiments at 677.0 and 680.8 nm. The original FLN spectra were saturated at the excitation wavelength; their difference there was therefore zero, and the spikes were artificially added to the Δ-FLN spectra to indicate the excitation wavelength. A copy of the black curve was shifted by 3.8 nm to the red to demonstrate that at longer wavelengths the shape of the Δ-FLN spectra is wavelength-independent. These spectra were fitted using the parameters reported in Table 1. Magenta and green dashed curves, respectively, are calculated Δ-FLN spectra for excitation wavelength of 670.7 nm and interpigment couplings J_{12} of 0 and 0.4 cm^{-1}.

depicts the Δ-FLN spectra for several excitation wavelengths; those obtained with excitation at the red edge of the absorption band directly represent the single-site spectrum, and in particular the phonon sideband, according to ref 24. The Δ-FLN spectrum is the difference between fluorescence line narrowing spectra before and after NPHB.[24,25] Since the ZPL contributions to the original FLN spectra were saturated, we used independently measured maximal depth of the zero-phonon hole to estimate $S_{phonon} \approx 0.7$, as in ref 18. The phonon sideband (PSB) is peaked at 24 cm^{-1}, also in agreement with ref 18. The detailed discussion on simulating Δ-FLN spectra in the presence of EET was presented in ref 26. Briefly, for long enough excitation wavelength (and in the absence of EET), the PSB of the Δ-FLN spectrum is nearly identical to the PSB of the single-site spectrum.[24,26] The PSBs in Figure 4 are sharp near the peak but have long tailing at higher frequencies and are not amenable to fitting with either a single log-normal curve[27] or a single half-Gaussian/half-Lorentzian curve as one-phonon profile for realistic values of S_{phonon}. As the focus of this work is not on the origins of this particular PSB shape, we used two components to produce a good enough single-site spectrum to be employed in subsequent modeling, one log-normal (S = 0.6) and one 24 cm^{-1} Lorentzian mode with S = 0.12. The log-normal part of the one-phonon profile is given by

$$l(\omega) = \frac{S}{\omega \sigma \sqrt{2\pi}} \exp\left(-\frac{(\ln(\omega/\omega_c))^2}{2\sigma^2} \right) \quad (1)$$

with ω_c being the cutoff frequency and σ being the standard deviation.[27] The parameters of the one-phonon profile are summarized in Table 1.

Table 1. SDF and Electron−Phonon Coupling Parameters for the Cyt b$_6$f Dimer (Long Lifetime Fraction)^a

SDF peak/ fwhm	lognormal PSB[27]; see eq 1: S, σ, ω_c, peak	24 cm^{-1} Lorentzian mode: S, width
14840/ 350 cm^{-1}	0.60, 0.8, 65 cm^{-1}, 37 cm^{-1}	0.12, 20 cm^{-1}

^{a}Local Chl *a* vibrations are according to ref 25.

The single-site spectrum includes ZPL and PSB as well as contributions due to localized Chl vibrations. Multiphonon processes are included according to ref 28 with modifications proposed in ref 29—in order to produce the *R*-phonon profile (R = 2, 3, ...), the one-phonon profile including log-normal $l(\omega)$ (eq 1), the 24 cm^{-1} Lorentzian mode, and the localized chlorophyll vibrations[25] was numerically convoluted with itself $R - 1$ times, without approximations. *R*-phonon profiles for R = 1, 2, ... were added together with the weighting factors $S^R/R!$. The zero-phonon profile is a Lorentzian normalized to $\exp(-\sum S)$, where the sum is over all phonons and localized vibrations.

The large gap between the peaks of the absorption and emission spectra can be explained neither by large electron−phonon coupling (it is moderate, see above) nor by invoking excitation energy transfer between two identical Chls of the Cyt b$_6$f dimer, by analogy with the trimeric FMO.[30] If the two Chls of the cytochrome dimer possessed identical true SDF, these would be peaked at about 669.5 nm. Following the logic of refs 26 and 30, one can calculate that the sub-SDF of the lower-energy pigments in the pair, corresponding to the HB action spectrum, would peak at about 671 nm and have the width of about 10 nm. In other words, in a scenario involving only the EET between two pigments with identical SDF, the emission spectrum and the HB action spectrum are supposed to be narrower than the absorption spectrum, not broader, as it was indeed observed for the Fenna−Matthews−Olson (FMO) complex,[30] for example. If EET is slow and some noticeable emission from the donor molecules is possible, the action and emission spectra would broaden (but not beyond the width of the absorption spectrum) and shift to the blue, not to the red. Besides, it appears that the absorption spectrum cannot be fitted employing one Gaussian SDF, as it has significant long-wavelength tailing. The fluorescence lifetime for the fraction of the pigments dominating the emission spectra, including FLN, is significantly longer than 250 ps as reported in refs 18 and 19. Figure 5 presents the dependence of the homogeneous line width on temperature for $\lambda_B \approx 677$ nm. For every temperature five holes of different depths were burned, and the extrapolation to zero hole depth was performed. It is clear that the holes burned below 4 K are narrower than the 250 ps lifetime[18,19] would permit (dashed horizontal line). The narrowest holes at 1.9 K correspond to the lifetime of about ~700 ps. There is no evidence or physical reason why this temperature dependence of the line width should level off right at 1.9 K, which is just the minimal temperature accessible in our setup; more likely the width follows the ~$T^{1.3}$ dependence
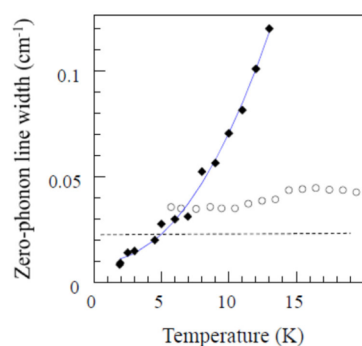
Figure 5. Black diamonds: temperature dependence of the homogeneous line width at around 677 nm. Five holes were burned at each temperature with varying illumination doses; results were extrapolated to zero hole depth. The horizontal dashed line corresponds to the 250 ps fluorescence lifetime reported in refs 18 and 19. The blue curve is a guide for the eye only. Also presented is the dependence of the homogeneous line width on thermocycling temperature for a 30% hole burnt at 5.5 K (open circles).

typical for amorphous solids and pigment−protein complexes below 5 K.[31−34] Therefore, the fluorescence lifetime of Chls dominating emission is likely longer than 700 ps, quite possibly a couple of nanoseconds, typical for Chls in a protein environment without additional quenching. A value of 2.5 ns was used for subsequent modeling. The blue curve in Figure 5 is a guide for the eye only. Due to somewhat limited temperature range we did not attempt fitting the data with a superposition of $\sim T^{1.3}$ and $\sim \exp(-\hbar\omega_{vib}/k_B T)$ terms, the latter being due to some low-frequency vibration possibly causing additional dephasing.[31−34]

In order to explain our observations we have to suggest that our cytochrome sample is somewhat heterogeneous. It is possible that in some fraction of our sample the fast quenching of the Chl excitations by the surrounding protein[18,19] does not occur. Thus, there may be four categories of Chls rather than two (higher-energy donor and lower-energy acceptor): quenchable donors, quenchable acceptors, unquenchable donors, and unquenchable acceptors, with the action spectrum representing mostly the latter. Quenchable pigments may still be in the majority and contribute the most to the absorption spectrum; their SDF appears to be narrower than that of the pigments that cannot be quenched by the protein. However, quenchable pigments do not contribute much to the emission. Ignoring possible contributions of quenched pigments to the emission completely, one can demonstrate that the Δ-FLN spectra depicted in Figure 4 are in good agreement with $S_{phonon} \approx 0.7$ and interpigment coupling of $J_{12} \approx 0.4$ cm^{-1} (dashed green curve). The magenta dashed curve depicts the spectrum predicted in the absence of EET. Note that the presence of EET is further confirmed by observing previously burned spectral holes in the shorter-wavelength Δ-FLN spectrum (blue curve in Figure 4, excitation wavelength 670.7 nm). This experimental Δ-FLN spectrum contains zero-phonon holes, pseudo-phonon sidebands, and NPHB antihole features. Such previously burned features in the Δ-FLN spectra would be impossible in the absence of EET.[26] One can also treat these results as a proof that the approach of ref 24 indeed predicts the Δ-FLN spectra correctly, i.e., that, due to double spectral selection, the Δ-FLN spectra do not contain significant pseudo-PSB contributions.
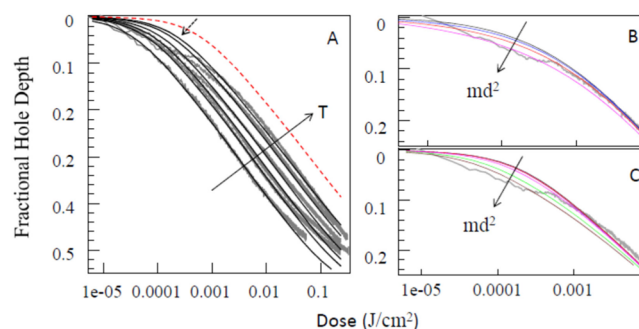

Figure 6. Frame A: HGK measured at 2, 5.5, 7.6, 9.6, 11.7, and 13.9 K (gray noisy curves) and their fits employing uniform λ-distribution with λ_{min} =8.2 and λ_{max} =12.2 and excited state TLS asymmetry of 4.5 cm^{-1} (smooth black curves). Dashed arrow indicates the region of discrepancy between experimental and modeling results, presumably due to the onset of hole burning via barrier-hopping. Dashed red line is the HGK curve calculated for T = 13.9 K and no temperature dependence of the tunneling rate (i.e., for large TLS asymmetry). Burn wavelength was 677 nm. Frame B: Effects of barrier hopping on HGK for Gaussian λ-distribution demonstrated for the 13.9 K HGK; md^2 = 0.1, 1.0, 1.1, and 1.2 × 10^{-46} kg·m^2. Frame C: Effects of barrier hopping on HGK for uniform λ-distribution demonstrated for the 13.9 K HGK; md^2 = 0.1, 1.0, 1.1, 1.2, 1.3, and 1.35 × 10^{-46} kg·m^2.

3.3. Protein Energy Landscapes and NPHB Mechanism.
Figure 6 presents the hole growth kinetics (HGK) curves obtained at several temperatures at λ_B around 677 nm. The HGK is the (fluorescence) signal decreasing with time while the laser is kept at fixed frequency, ω_B. In terms of the hole burning master equation for the postburn absorption spectrum

$$D(\Omega, t) = \int d\omega \, L(\Omega - \omega) G(\omega) \int d\lambda \, f(\lambda)$$
$$\int d\alpha \, \frac{3}{2} \sin\alpha \, \cos^2\alpha \, e^{-P\sigma\phi(\lambda)L(\omega_B - \omega)t\cos^2\alpha} \tag{2}$$

the HGK curves in Figure 6 represent $D(\omega_B, Pt)$ normalized to $D(\omega_B, 0) = 1$. $G(\omega)$ is the SDF, $L(\omega)$ is the single-site spectrum shape with area normalized to unity on the frequency scale, ω_B is the excitation frequency, t is the burn time, P is the photon flux, σ is the integral absorption cross-section, and ϕ is the NPHB yield given by

$$\phi(\lambda) = \frac{\Omega_0 \exp(-2\lambda)}{\Omega_0 \exp(-2\lambda) + \tau_{fl}^{-1}} \tag{3}$$

Ω_0 is the attempt frequency on the order of 10^{12} Hz. It determines how often the system approaches the barrier through which it may tunnel; the value is believed to be on the order of the typical vibration frequencies (see Discussion section). For the sake of easy comparison with the results obtained for glasses[35−37] and other pigment−protein complexes[7−9] here we again use $\Omega_0 = 7.6 \times 10^{12}$ Hz, admittedly somewhat exaggerated, unless specified otherwise. Lambda is the tunneling parameter, whose distribution is $f(\lambda)$. It is related to the barrier heights according to $\lambda = d(2mV)^{1/2}/\hbar$, where V is the barrier height, d is the shift along the generalized coordinate, and m is the effective mass of the entity rearranging during conformational change. Some of these quantities can be visualized with the help of Figure 1. The parameters of the excited state λ-distribution can be determined by comparing experimental and simulated HGK. τ_{fl} is the fluorescence lifetime in the absence of EET, and α is the angle between laser polarization and transition dipole moment vector of the

pigment. Isotropic pigment orientation is assumed. The denominator of eq 3, in principle, can contain also the characteristic EET time. However, on the red edge of the band the absorption is dominated by the acceptor molecules, which are incapable of further downhill EET (two longer-wavelength Δ-FLN spectra in Figure 4 are identical).

As can be seen, the hole burning process is gradually slowing down with temperature. This slowdown is expected due to the increase of the homogeneous line width with temperature depicted in Figure 5, accompanied by some increase of $S_{phonon}(T)$.[28] Both effects lead to the decrease of the peak absorption cross-section of the ZPL in the exponential in eq 2. However, unlike in CP43, at the higher temperatures the burning is somewhat faster than would follow from the above effects alone; see dashed red line in Figure 6A. These discrepancies can be explained if one includes into consideration the temperature dependence of the rate of phonon-assisted tunneling involving the shift to a deeper well of the energy landscape and an increase of the scattered phonon energy (i.e., "downhill tunneling"; $1 \rightarrow 2$ transition in Figure 1) $\Omega_0 \exp(-2\lambda)(n(\Delta) + 1)$ that is slightly increasing with temperature. $n(\Delta) = 1/(\exp(\Delta/k_B T) - 1)$ is the population number for phonons employed in phonon-assisted tunneling. Better global fit to all HGK curves can be achieved for TLS asymmetry $\Delta \approx 4.5$ cm^{-1}. For CP43[9] the average excited state TLS asymmetry apparently was larger, and thus the temperature dependence of the tunneling rate was less prominent.

The parameters of the λ-distribution obtained from the fit to the HGK curves are similar to those reported for CP43[9] and other protein−chlorophyll complexes[7,8] under similar conditions and assumptions. Namely, if $f(\lambda)$ is Gaussian and the temperature dependence of the tunneling rate is properly taken into account, $\lambda_0 = 10.25 \pm 0.10$ and $\sigma_\lambda = 1.3 \pm 0.1$ is obtained from the fits to the HGK for a fluorescence lifetime of 2.5 ns. This could be compared to $\lambda_0 = 10-11$ and $\sigma_\lambda = 1.3-2.0$ observed for other protein−chlorophyll complexes[7−9] and to $\lambda_0 \approx 8$ and $\sigma_\lambda \approx 1$ observed for aluminum phtalocyanine tetrasulfonate or free base phthalocyanine in a number of simple organic glasses and hyperquenched glassy water.[35−37]

In order to determine the qualitative shapes of the $\lambda-$ or barrier height distributions involved in NPHB and fixed-temperature hole recovery, we followed the logic of ref 9 and performed joint analysis of the 5.5 K HGK data in Figure 5 and the 5.5 K recovery data presented in Figure 7A. Note that the holes that were initially shallower are recovering relatively faster. The difference in recovery of 20%- and 42%-deep holes is close to the maximal possible value predicted for the case of the perfect spectral memory (see Discussion). In other words, recovery at 5.5 K is strongly dominated by the burned pigment−protein systems returning to the preburn configuration characterized by the original transition frequency of the pigment. The recovery curves were fairly repeatable (not shown). We also note that the recovery rate was independent of temperature between 5 and 10 K and slowed down somewhat at 13 K (not shown). As any process responsible for the recovery has to accelerate with temperature, this indicates the increase of the NPHB rate with temperature (NPHB occurring while measuring with the small read intensity is slowing down the *apparent* recovery).

The presence of spectral memory justifies the use, for hole recovery modeling, of partial λ-distributions actually encoded into the holes, which are drastically different in the cases of Gaussian and uniform (corresponding to $\sim 1/\sqrt{V}$-shaped
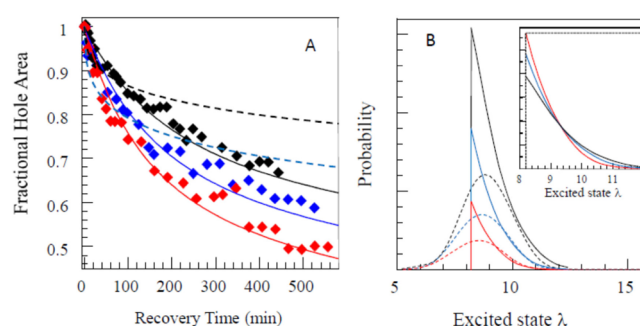

Figure 7. Frame A. Diamonds—measured recovery of 42%-deep (black), 31%-deep (blue), and 20%-deep (red) holes at 5.5 K. Solid curves of matching colors—fits to the recovery curves obtained starting from uniform λ-distribution. Dashed black and blue curves— poor fits obtained starting from a Gaussian λ-distribution. See text for more details. Frame B: Partial λ-distributions actually encoded into the spectral holes for 20% (red), 30% (blue), and 40% (black) holes and the same parameters as used for fitting HGK curves. Dashed curves— partial λ-distributions obtained for Gaussian full true λ-distribution. Solid curves were obtained for uniform true full λ-distribution. The inset in Frame B depicts the same partial excited state λ-distributions as in the main Frame B, but renormalized to the same area under the curve. The dashed box represents the full true λ-distribution.

barrier distribution) full true λ-distributions.[9] The HGK data in Figure 6A was fitted also under the assumption of the uniform true full distribution of λ between $\lambda_{min} = 8.2$ and $\lambda_{max} = 12.2$. Then partial distributions of λ actually contributing to the nonsaturated holes for both types of full true λ-distributions were calculated as in ref 9, and simulated recovery curves were compared with the experiment. Figure 7B depicts the partial λ-distributions encoded into the spectral holes of various fractional depths under the assumptions of uniform (solid lines) and Gaussian (dashed lines) true full λ-distributions. The inset depicts partial distributions in the uniform (box-like) true full distribution case, normalized to the same area under the curve. As the relative contribution of smaller-λ systems is larger for shallower holes, these holes are expected to recover faster. Note that we also made an assumption that the magnitudes of the ground state barriers that are crossed during recovery are proportional to the magnitudes of the excited state barriers. All recovery curves calculated for the uniform λ-distribution (black, red, and blue solid smooth curves in Figure 7) were produced utilizing the same scaling factor $k = \lambda_{ground}/\lambda_{excited} = 2.35 \pm 0.01$. Thus, barriers in the ground state are $2.35^2 = 5.5$ times higher than in the excited state, and the magnitudes of the ground and excited state barriers within one pigment−protein system are likely indeed well-correlated. Dashed curves were obtained starting from a Gaussian true full λ-distribution. As can be seen from the comparison between experimental and calculated recovery curves, the full true ground-state λ-distribution is more likely uniform and not Gaussian (although the fit is somewhat imperfect for the uniform distribution as well). In the case of a Gaussian distribution faster initial recovery and slower recovery after a couple of hours are predicted (dashed curves).

Returning to Figure 6, one can also notice that even when the weak temperature dependence of the tunneling rate is taken into account, the hole burning above 10 K is somewhat too fast in the beginning, compared to the calculated HGK; see dashed arrow in Frame A. This effect is consistently present in several HGK curves in Figure 6 and for both assumptions about the true λ-distribution shape. This may indicate an onset of an

additional HB mechanism. Given the arguments presented above and justifying the use of the downhill tunneling approximation, it is unlikely that this additional process is uphill tunneling. Besides, any tunneling rate would increase with temperature uniformly for all λ, without any preference for the smaller ones that characterize individual systems that are the first to burn. The tunneling rate is a product of λ-dependent and temperature-dependent terms containing $n(\Delta)$, with asymmetry Δ being independent of λ. On the other hand, barrier hopping would indeed turn on selectively for smaller-λ systems first.[9] Evidence of both barrier-hopping and tunneling was found in single LH2 complexes between 5 and 18 K.[38] One can use the HGK curves to estimate the md^2 parameter of the entity involved in the conformational changes. Barrier hopping and tunneling contributions to hole burning are comparable when $\exp(-2\lambda) \approx \exp(-V/k_BT)$ or $\lambda \approx \lambda^2\hbar^2/2md^2k_BT$. Contribution from barrier-hopping to the HB yield was incorporated into the hole burning modeling software and improved (but not perfect) agreement between HGK simulations and experiment was achieved. We need to mention, though, that this barrier hopping correction worked better when Gaussian λ-distribution was employed (Figure 6B versus Figure 6C), in disagreement with the analysis of the recovery data in Figure 7. Best agreement can be achieved for $md^2 = 1.15 \times 10^{-46}$ kg·m^2. This value is only 15% larger than the upper limit of $md^2 = 1.0 \times 10^{-46}$ kg·m^2 reported for CP43.[9] While in the case of a Gaussian λ-distribution predominantly the beginning of the HGK was accelerated, for uniform λ-distribution the acceleration was more present for all stages of HGK. This makes perfect sense if one looks at Figure 7B: Gaussian λ-distributions have the tails protruding toward smaller λ than the λ_{min} of the uniform λ-distribution, and a small percentage of systems characterized by these small λ burn more exclusively in the beginning of the burning process. In contrast, for uniform λ-distribution the smallest-λ systems are characterized by larger $\lambda \approx 8.2$ and are less prone to barrier-hopping than the systems with $\lambda < 8$ from the Gaussian scenario.

Figure 8A depicts the recovery of a 30%-deep spectral hole upon thermocycling (black diamonds). It also contains the fixed-temperature 5.5 K recovery data and its fit (blue diamonds and solid line) and the results of modeling of thermocycling-induced recovery using the same ground state λ-distribution parameters as obtained above for the fixed-temperature hole recovery, for several different md^2 values from 1.0×10^{-46} to 1.9×10^{-46} kg·m^2 (dashed curves). The horizontal axis of Figure 8A presents time rather than temperature; the temperature is introduced indirectly via employing the actual temperature vs time profile used in the thermocycling experiment. Some temperatures are indicated next to their respective data points. Initial recovery (the first 2 h, at temperatures below ~11 K; the first hour was spent at 5.5 K without thermocycling) follows the same path as in Figure 7A. As can be seen from the comparison of experimental data and modeling results (dashed curves) experimental data is compatible with $md^2 \leq 1.4 \times 10^{-46}$ kg·m^2, but, as for CP43,[9] there appears to be an additional spectral memory-less recovery channel[9] (see additional discussion below). Larger md^2 values would not be allowed; crossing of the experimental and simulated curves (shown for $md^2 = 1.9 \times 10^{-46}$, brown dashed line) would mean that the additional recovery is partially reversed with the increase of temperature, which is
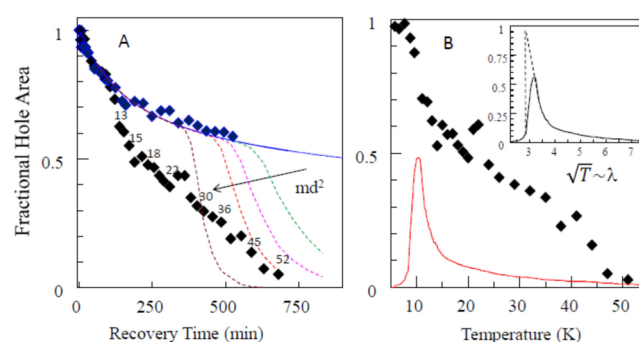

Figure 8. Frame A: The recovery of a 30%-deep hole upon thermocycling (black diamonds), compared to recovery at 5.5 K (blue diamonds) and its fit (blue solid line), as well as recovery curves calculated based on real temperature change profile for several different values of md^2 (dashed lines); md^2 is increasing from 1.0 (green) to 1.15 (magenta) to 1.3 (red) to 1.9×10^{-46} kg·m^2 (brown) in the direction of the arrow. Numbers above some of the data points indicate respective temperatures in Kelvin. Frame B: Black diamonds: recovery due to thermocycling corrected for recovery that would occur at 5.5 K anyway. Red curve: the distribution of barriers V corresponding to the recovery data. Inset: distribution as a function of $\sqrt{T} \sim \sqrt{V} \sim \lambda$.

unphysical. Values of md^2 smaller than 1.0×10^{-46} kg·m^2 are, however, definitely possible.

Figure 8B shows recovery due to thermocycling alone, after taking corrections for recovery occurring anyway at 5.5 K. The barrier distribution involved can be obtained noticing that the fraction of systems remaining unrecovered after cycling to T_{max} is

$$f = 1 - \int_0^{V(T_{max})} g(V)\, dV,$$

with $V(T_{max}) = k_B T_{max} \ln(t_{max}\Omega_0)$ (4)

where $g(V)$ is distribution of barrier heights, $t_{max} \approx 60$ s is time spent at the peak cycle temperature T_{max}, and Ω_0 is the attempt frequency.[39] It is clear that $g(V)$ obtained from experimental data and sketched in Figure 8B is not Gaussian and resembles the results of refs 10−12, where the $g(V) \sim 1/\sqrt{V}$ barrier distribution was deduced. A small plateau in the experimental data (diamonds) at the lowest temperatures can be explained by the smallest-barrier systems recovering due to tunneling during the first hour at burn temperature, before thermocycling started. The inset depicts the approximate shape of the λ-distribution involved in thermocycling-induced recovery. Dashed lines sketch the part of the λ-distribution (~20% of the spectral hole area) that recovered during the first hour, before thermocycling was started. The shape of this λ-distribution resembles the shapes of the partial λ-distributions encoded into the holes in the case of perfect spectral memory and uniform true full λ-distribution (solid curves in Figure 7B). It is significantly different from either nearly Gaussian shapes (dashed lines in Figure 7B) or from the box-like shape expected in the case of the uniform λ-distribution but no spectral memory (i.e., when partial barrier or λ-distributions are identical to the full true ones).

Finally, we note that the hole broadens rather slowly upon thermocycling, and the width after cycling to temperatures exceeding 10 K is clearly smaller than the widths of the holes burned at respective temperatures (open circles in Figure 5). This indicates fairly slow spectral diffusion with small ($\ll 1$

cm^{-1}) spectral shifts[3,40,41] below 20 K. Overall, the dependence of the hole width on the maximal temperature of the cycle resembles that reported for phycobilisomes,[41] except the linear (within experimental errors) increase of the hole width persists at least to 45 K when the hole is nearly recovered and the ~$T^{3/2}$ term[41] is not observed. Thus, reliable determination of the md^2 parameter for the entities whose conformational changes are responsible for the hole broadening in Cyt b$_6$f is unfortunately impossible. We can only conclude that it is smaller than 4.3 × 10^{-46} kg·m^2 or 26 m_{proton}·Å^2 observed for phycobilisomes.[41]

4. DISCUSSION

4.1. Evidence of EET and Intactness of the Cyt b$_6$f Samples.
Good agreement between interpigment coupling values obtained from the structural data and from simulations of the Δ-FLN spectra, as well as other evidence of EET (holes in the Δ-FLN spectra in Figure 4), suggest that Chl molecules not exhibiting fast quenching and dominating fluorescence and fluorescence excitation spectra are not randomly nonspecifically bound to the protein or released into the buffer−glycerol solution. They are likely still located within their designated protein pockets, but the fast quenching mechanism is turned off. Interestingly, the same arguments must be to a significant degree true also for the monomeric Cyt b$_6$f sample reported in ref 18; otherwise, the relationship between absorption and emission spectra for that sample would be significantly different. In particular, the emission spectrum would have approximately the same width as the absorption spectrum. It is possible that quenching of Chl excitations is associated with conformational changes whose barriers are too high to cross at cryogenic temperatures. (The 250 ps lifetime[18,19] was reported at room temperature.) The hole burning and recovery rates are also typical for pigment−protein complexes and not for pigments in organic glasses. Summarizing, we are confident that lower-energy higher fluorescence yield Chls of the Cyt b$_6$f dimer are suitable probes for protein dynamics (rather than surrounding solvent dynamics) exploration.

4.2. Protein Energy Landscapes—Details of the NPHB and Recovery Mechanism.
The weak temperature dependence of the HB yield (or no such dependence in the case of CP43[9]) is not compatible with the weighted sum of downhill and uphill tunneling processes corresponding to the thermal equilibrium or even to the situation with equal probabilities of uphill and downhill tunneling (flash-frozen higher-temperature equilibrium). In both these cases the expected temperature dependence would be stronger than observed. Figure 9 shows expected temperature dependence of the tunneling rate in all these scenarios. Downhill tunneling (black curve, a) has the smallest ratio of tunneling rates at $T > 0$ and $T = 0$.

The predominance of the downhill tunneling as the hole burning mechanism reflects an unnatural antiequilibrium situation where the majority of the deepest wells of the TSL are not occupied. Thus, explaining the results presented here and for CP43 requires invoking, for proteins, of an analogue of the Shu−Small NPHB mechanism.[42] In this mechanism, the excited state of the TLS involving the pigment (analogue of the "extrinsic TLS" in glasses) gets poised for downhill tunneling due to the diffusion of free volume associated with excitation-induced transitions in the "intrinsic" TLS. Our ability to burn zero-phonon holes to maximal depth allowed by electron−phonon coupling S_{phonon} (~50% for S_{phonon} = 0.7) even below 2 K further confirms the presence of the Shu−Small mechanism[42]
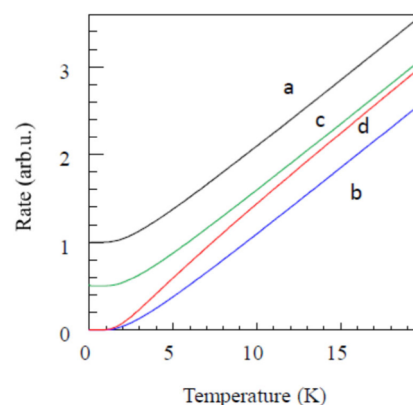

Figure 9. Temperature dependence of NPHB rate for downhill tunneling (black, a), uphill tunneling (blue, b), average of uphill and downhill tunneling flash-frozen higher-temperature equilibrium (green, c), and the weighted average of uphill and downhill tunneling at thermal equilibrium at the respective temperature (red, d).

of NPHB in Cyt b$_6$f (and CP43, where up to 70% zero-phonon holes were possible with S_{phonon} = 0.35).

The results of the joint analysis of the HGK and fixed-temperature recovery data suggest the presence of nearly perfect spectral memory. In the absence of spectral memory the holes of different depths would recover with the same relative speed, contrary to what is shown in Figure 7A. Note that the "lack of spectral memory" should not be understood as each system possessing an infinite number of available conformational substates. It merely means that the hole may be filled by the absorption of the molecules which were not in resonance with the laser prior to burning. Let us discuss a somewhat oversimplified no-memory model where hole depth is proportional to the hole area and where there are N molecules absorbing at any wavelength around the burn wavelength before burning and assume that all protein/pigment systems are M-substate systems, so every system can be in one of M different conformational substates. ($M = 2$ corresponds to a classical TLS, two level system.) Thus, there are total MN molecules in the ensemble, which have one conformational substate (occupied or unoccupied) resonant with the laser. Suppose the rate of spontaneous switching between any two substates is k and that the current number of molecules still at resonance after burning is $P(t)$. Then the number of molecules out of resonance which potentially can switch to resonance would be $MN − P(t)$. Division by $M − 1$ in the subsequent equation reflects the fact that only one out of $M − 1$ wells available for transitions from an out-of resonance substate is the resonant one.

$$\frac{dP(t)}{dt} = k\frac{(MN - P(t))}{M - 1} - kP(t) = k(N - P(t))\left[\frac{M}{M - 1}\right]$$

$$U(t) = N - P(t)$$

$$U(t) = U(0)\exp\left(-k\left[\frac{M}{M - 1}\right]t\right)$$

Here $U(t)$ is the number of molecules that are removed from the resonance at time t and $U(0)/N$ is the fractional hole depth immediately after burning. While plotting normalized recovery data as in Figure 7A, we essentially are plotting $U(t)/U(0)$. In the absence of spectral memory this quantity does not depend on the initial fractional hole depth regardless of the number of

available substates M, at least for simple topologies of the protein energy landscape, and including $M = 2$.

Next we will address the issue of the additional thermocycling-induced recovery mechanism that cannot be accounted for using the same barrier distribution as manifests during the fixed-temperature recovery (see Figure 8). Modeling of NPHB and recovery processes employing multiwell energy landscapes of different shapes and in the samples in or out of thermodynamic equilibrium[43] does not yield anything resembling the observed gradual recovery upon thermocycling. Since this additional recovery mechanism cannot be explained within the model involving even the realistic imperfect spectral memory, the respective distribution of the barriers has to be the true full barrier distribution for another tier of the protein energy landscape, as was suggested for CP43.[9] Yet the λ-distribution sketched in the inset of Figure 8B looks a lot like the partial distributions encoded into the nonsaturated holes in the case spectral memory is present (solid curves in Figure 7B), except for the incorrect ratio of $\lambda_{ground,min}$ to $\lambda_{ground,max}$. In retrospect, this might have been true for CP43[9] as well, except the in the case when both true full and partial λ-distributions were close to Gaussian it was more difficult to notice.

At this point one may ask if it is possible to find a set of parameters that would explain all HGK, fixed temperature recovery and thermocycling results without invoking any additional tiers of the energy landscape and/or recovery channels. From the data in the inset of Figure 8B it follows that $\lambda_{ground,max} \approx 2.6\lambda_{ground,min}$. On the other hand, in order to explain both HGK and fixed-temperature recovery, one still has to assume that $\lambda_{ground,max} = (\lambda_{exc,max} - \lambda_{exc,min}) \cdot k + \lambda_{ground,min} \approx 9.4 + \lambda_{ground,min}$, where the scaling factor $k = \lambda_{ground}/\lambda_{exc} = 2.35 \pm 0.01$ (see above). From here $\lambda_{ground,min} \approx 5.9$, $\lambda_{ground,max} \approx 15.3$, $\lambda_{exc,min} \approx 2.5$, and $\lambda_{exc,max} \approx 6.5$. The average λ_{exc} is about 4.5. These unusually low values of λ can still be in agreement with the fits to the HGK and fixed temperature recovery data if the attempted frequency is reduced accordingly by a factor of about $(e^2)^{10.2-4.5} \approx 9 \times 10^4$, to as low as 85 MHz. Then one can utilize the data in Figure 8B for determination of md^2 using the method outlined in Love et al.,[39] i.e., assuming that both fixed-temperature and thermocycling-induced recovery reflect one and the same barrier distribution. With reduced attempt frequency, $\ln(t_{max}\Omega_0) \approx 22$, $V_{max,ground} \approx 790$ cm^{-1}, and $md^2 \approx 0.8 \times 10^{-46}$ kg·m^2. This value is again very close to those presented above and for CP43.[9] For $md^2 \approx 1 \times 10^{-46}$ kg·m^2 (or $6m_{proton} \cdot Å^2$) if tunneling involved a proton, the distance d would be 2.44 Å, which is a typical hydrogen bond length. However, in the case of tunneling within a sufficiently long hydrogen bond yielding double-well potentials, values of d several times smaller than the hydrogen bond length were suggested.[44,45] For a methyl or a hydroxyl group $md^2 = 1.0 \times 10^{-46}$ kg·m^2 would lead to $d = 0.63$ or 0.59 Å, respectively. These numbers are comparable to deviations of the soft regions of protein from equilibrium positions according to X-ray scattering.[46,47] If the above arguments in favor of the reduced attempt frequency are correct, they would further support larger m and smaller d options for the tunneling entity. However, it is unclear how one could justify an attempt frequency four orders of magnitude lower than the typical vibration frequencies. It was estimated, based on the typical values of protein compressibility,[48] that the chromophore-to-TLS distance $R \sim 1$ nm, $\Delta R/R \sim 10^{-3}$, and the net charge of the shifting entity is equal to the charge of a proton correspond to spectral shifts of several wavenumbers.[40] Thus, $d \approx \Delta R$ can

be as low as 0.01 Å for NPHB to still be observable in the case of proton tunneling. However, respective increase of m by a factor of $\sim 10^4$ would result in an attempt frequency decrease by $\sim 10^2$ only and would be incompatible with tunneling entities being protons.

In the most general terms, reduction of the attempt frequency could result from the cooperative effects, involving the whole network of weak interactions holding the protein together. One possible way to look at the cooperative effects reducing the attempt frequency employs the quantum-mechanical analogue of beats. Imagine multiple oscillators with similar microscopic structure and similar but nonidentical frequencies. If initiating a conformational change requires all these oscillators to be in phase simultaneously, this condition will be satisfied much less frequently than the period of each individual oscillator and the effective attempt frequency will be reduced. The cooperative rearrangements could include movements of either protons (explaining the sensitivity of Photosystem I (PSI) dynamics to deuteration[49]) or other, more massive, entities, or both. Of course, in this scenario m and d become disconnected from the actual mass and displacement of some one particular entity. Cooperative effects are also in line with the presence of the Shu−Small NPHB mechanism[42] in proteins as suggested above, with some additional conformational changes poising the "extrinsic TLS" for downhill tunneling. The coupling between multiple structural features of the protein at cryogenic temperatures was inferred from the hole broadening experiments in protoporphyrin−IX-substituted myoglobin.[50] Another likely example of cooperative effects in spectral dynamics of pigment−protein complexes is the switching between different EET pathways in PSI.[51]

Is there a way to reconcile the observations for Cyt b_6f and CP43 in terms of the qualitative shapes of the barrier distributions? A superposition of Gaussian and $\sim 1/\sqrt{V}$ terms was observed in a thermocycling experiment on phycobilisomes.[12] The results presented here also may be explained by assuming complex shape of the true full λ-distribution which is roughly 85% uniform (box-like) and 15% Gaussian. (This would account for faster initial stages of burning and recovery.) Note that it is not clear why distinct λ_{min} and λ_{max} (V_{min} and V_{max}) should exist in an amorphous system. One could think of the true λ-distribution functions with a flattened center and relatively narrow tails approaching zero asymptotically. If such a complex distribution is narrow enough, the hole behavior may be dominated by the Gaussian-like tails, while if such a distribution is broad, flat central part would play an increasing role. It remains to be seen (via performing similar experiments on other pigment−protein complexes such as LH2[3,7,33] (an antenna pigment−protein complex from purple bacteria) or CP29[8,25] (one of the antenna pigment−protein complexes of Photosystem II), for example, if there is a correlation between the degree of disorder (larger inhomogeneous width and/or larger overall width of the λ-distribution) and the tendency of the holes to obey uniform λ-distribution rather than a Gaussian one. Alternatively, one can speculate that Gaussian barrier distributions of CP43 are a direct result of a significant excitonic character of the lowest-energy state[15,16] (A-state[31]). In this scenario each Chl contributing to the A-state experiences box-like or nearly box-like distribution of λ, but the weighted sum of several such distributions may look Gaussian enough. (Imagine a typical histogram approximated by the normal distribution from an introductory probability course.) Confirming any of these scenarios will have implications for

determining the limits of applicability of the theories of amorphous solids at low temperatures to proteins.

5. CONCLUDING REMARKS

The results presented here indicate that the (full true) barrier distributions for the energy landscape tier involved in NPHB in Cyt b_6f are proportional to $1/\sqrt{V}$. Cytochrome results are thus the exact opposite of what was reported in the case of CP43[9] and similar to the distributions observed in thermocycling experiments in glasses.[10−12] As discussed above, it is very unlikely that Chls explored in this study were released by the partially denatured protein and surrounded by the glassy solvent. This would contradict the presence of the EET between the two Chls of the dimer with the rate following from the structure data,[17] as demonstrated in Figure 4. Quantitatively, the parameters of the excited and ground-state distributions are also typical for pigment−protein complexes and not for pigments in organic glasses.[35−37] Thus, the suggestion voiced in the Introduction, that all amorphous solids or at least all proteins may possess only Gaussian barrier distributions,[9] was not confirmed. Several different estimates for the md^2 parameter characterizing tunneling entities were presented. They are consistently grouped around $md^2 = 1.0 \times 10^{-46}$ kg·m², indicating that entities involved in the conformational changes responsible for NPHB are either protons or small atom groups of the protein side chains. A tempting explanation alternative to attributing the NPHB and recovery to the tunneling of some one particular entity involves cooperative effects resulting in a significant decrease of the attempt frequency. Searching for detailed understanding, on an atomic level, of factors possibly leading to the attempt frequencies as low as 100 MHz constitutes an additional interesting avenue of future research.

■ AUTHOR INFORMATION

Corresponding Author
*E-mail: valter.zazubovits@concordia.ca.

Notes
The authors declare no competing financial interest.

■ ACKNOWLEDGMENTS

■ REFERENCES

(1) Frauenfelder, H.; Sligar, S. G.; Peter, G. The Energy Landscapes and Motions of Proteins. *Science* **1991**, *254*, 1598−1603.

(2) Fenimore, P. W.; Frauenfelder, H.; McMahon, B. H.; Young, R. D. Proteins are Paradigms of Stochastic Complexity. *Physica A* **2005**, *351*, 1−13.

(3) Hofmann, C.; Aartsma, T. J.; Michel, H.; Köhler, J. Direct Observation of Tiers in the Energy Landscape of a Chromoprotein: A Single-molecule Study. *Proc. Natl. Acad. Sci. U.S.A.* **2003**, *100*, 15534−15538.

(4) Berlin, Y.; Burin, A.; Friedrich, J.; Köhler, J. Low Temperature Spectroscopy of Proteins. Part II: Experiments with Single Protein Complexes. *Phys. Life Rev.* **2007**, *4*, 64−89.

(5) Berlin, Y.; Burin, A.; Friedrich, J.; Köhler, J. Spectroscopy of Proteins at Low Temperature. Part I: Experiments with Molecular Ensembles. *Phys. Life Rev.* **2006**, *3*, 262−292.

(6) Jankowiak, R.; Hayes, J. M.; Small, G. J. Spectral Hole-Burning Spectroscopy in Amorphous Molecular Solids and Proteins. *Chem. Rev.* **1993**, *93*, 1471−1502.

(7) Grozdanov, D.; Herascu, N.; Reinot, T.; Jankowiak, R.; Zazubovich, V. Low-Temperature Protein Dynamics of the B800 Molecules in the LH2 Light-Harvesting Complex: Spectral Hole Burning Study and Comparison with Single Photosynthetic Complex Spectroscopy. *J. Phys. Chem. B* **2010**, *114*, 3426−3438.

(8) Herascu, N.; Najafi, M.; Amunts, A.; Pieper, J.; Irrgang, K.-D.; Picorel, R.; Seibert, M.; Zazubovich, V. Parameters of the Protein Energy Landscapes of Several Light-Harvesting Complexes Probed via Spectral Hole Growth Kinetics Measurements. *J. Phys. Chem. B* **2011**, *115*, 2737−2747.

(9) Najafi, M.; Herascu, N.; Seibert, M.; Picorel, R.; Jankowiak, R.; Zazubovich, V. Spectral Hole Burning, Recovery, and Thermocycling in Chlorophyll−Protein Complexes: Distributions of Barriers on the Protein Energy Landscape. *J. Phys. Chem. B* **2012**, *116*, 11780−11790.

(10) Köhler, W.; Friedrich, J. Distribution of Barrier Heights in Amorphous Organic Materials. *Phys. Rev. Lett.* **1987**, *59*, 2199−2202.

(11) Köhler, W.; Meiler, J.; Friedrich, J. Tunneling Dynamics of Doped Organic Low-temperature Glasses as Probed by a Photophysical Hole-burning System. *Phys. Rev. B* **1987**, *35*, 4031−4037.

(12) Köhler, W.; Friedrich, J.; Scheer, H. Conformational Barriers in Low-temperature Proteins and Glasses. *Phys. Rev. A* **1988**, *37*, 660−662.

(13) Anderson, P. W.; Halperin, B. I.; Varma, C. M. Anomalous Low-temperature Thermal Properties of Glasses and Spin Glasses. *Philos. Mag.* **1972**, *25*, 1−9.

(14) Phillips, W. A. Tunneling States in Amorphous Solids. *J. Low Temp. Phys.* **1972**, *7*, 351−360.

(15) Dang, N. C.; Zazubovich, V.; Reppert, M.; Neupane, B.; Picorel, R.; Seibert, M.; Jankowiak, R. The CP43 Proximal Antenna Complex of Higher Plant Photosystem II Revisited: Modeling and Hole Burning Study. I. *J. Phys. Chem. B* **2008**, *112*, 9921−9933.

(16) Reppert, M.; Zazubovich, V.; Dang, N. C.; Seibert, M.; Jankowiak, R. Low-Energy Chlorophyll States in the CP43 Antenna Protein Complex: Simulation of Various Optical Spectra. II. *J. Phys. Chem. B* **2008**, *112*, 9934−9947.

(17) Yamashita, E.; Zhang, H.; Cramer, W. A. Structure of the Cytochrome b_6f complex: Quinone Analogue Inhibitors as Ligands of Heme cn. *J. Mol. Biol.* **2007**, *370*, 39−52.

(18) Peterman, E. J.; Wenk, S.-O.; Pullerits, T.; Pålsson, L.-O.; van Grondelle, R.; Dekker, J. P.; Rogner, M.; van Amerongen, H. Fluorescence and Absorption Spectroscopy of the Weakly Fluorescent Chlorophyll *a* in Cytochrome b_6f of *Synechocystis* PCC6803. *Biophys. J.* **1998**, *75*, 389−398.

(19) Dashdorj, N.; Zhang, H.; Kim, H.; Yan, J.; Cramer, W. A.; Savikhin, S. The Single Chlorophyll *a* Molecule in the Cytochrome b_6f Complex: Unusual Optical Properties Protect the Complex against Singlet Oxygen. *Biophys. J.* **2005**, *88*, 4178−4187.

(20) Yan, J.; Dashdorj, N.; Baniulis, D.; Yamashita, E.; Savikhin, S.; Cramer, W. A. On the Structural Role of the Aromatic Residue Environment of the Chlorophyll *a* in the Cytochrome b_6f Complex. *Biochemistry* **2008**, *47*, 3654−3661.

(21) Romanowska, E. In *Photosynthesis Research Protocols*; Methods in Molecular Biology 684; Carpentier, R., Ed.; Springer: 2011; pp 53−64.

(22) Pierre, Y.; Breyton, C.; Kramer, D.; Popot, J. L. Purification and Characterization of the Cytochrome b_6f Complex from *Chlamydomonas reinhardtii*. *J. Biol. Chem.* **1995**, *270*, 29342−29349.

(23) Zharkov, I. P.; Ivashchenko, A. N.; Pogrebnjak, S. V.; Safronov, V. V. Optimization of Temperature Control in Liquid Flow Cryostats. *Ukr. J. Phys.* **2010**, *55*, 350−355.

(24) Reppert, M.; Naibo, V.; Jankowiak, R. Accurate Modeling of Fluorescence Line Narrowing Difference Spectra: Direct Measurement of the Single-site Fluorescence Spectrum. *J. Chem. Phys.* **2010**, *133*, 014506-1−014506-9.

(25) Rätsep, M.; Pieper, J.; Irrgang, K.-D.; Freiberg, A. Excitation Wavelength-dependent Electron-phonon and Electron-vibrational

Coupling in the CP29 Antenna Complex of Green Plants. *J. Phys. Chem. B* **2008**, *112*, 110−118.

(26) Zazubovich, V. Fluorescence Line Narrowing and Δ-FLN Spectra in the Presence of Excitation Energy Transfer between Weakly Coupled Chromophores. *J. Phys. Chem. B* **2014**, *118*, 13535−13543.

(27) Kell, A.; Feng, X.; Reppert, M.; Jankowiak, R. On the Shape of the Phonon Spectral Density in Photosynthetic Complexes. *J. Phys. Chem. B* **2013**, *117*, 7317−7323.

(28) Hayes, J. M.; Lyle, P. A.; Small, G. J. A Theory for the Temperature Dependence of Hole-Burned Spectra. *J. Phys. Chem.* **1994**, *98*, 7337−7341.

(29) Reppert, M.; Kell, A.; Pruitt, T.; Jankowiak, R. Comments on the Optical Lineshape Function: Application to Transient Hole-burned Spectra of Bacterial Reaction Centers. *J. Chem. Phys.* **2015**, *142* (094111), 1−8.

(30) Herascu, N.; Kell, A.; Acharya, K.; Jankowiak, R.; Blankenship, R. E.; Zazubovich, V. Modeling of Various Optical Spectra in the Presence of Slow Excitation Energy Transfer in Dimers and Trimers with Weak Interpigment Coupling: FMO as an Example. *J. Phys. Chem. B* **2014**, *118*, 2032−2040.

(31) Jankowiak, R.; Zazubovich, V.; Rätsep, M.; Matsuzaki, S.; Alfonso, M.; Picorel, R.; Seibert, M.; Small, G. J. The CP43 Core Antenna Complex of Photosystem II Possesses Two Quasi-Degenerate and Weakly Coupled Q_y-Trap States. *J. Phys. Chem. B* **2000**, *104*, 11805−11815.

(32) Rätsep, M.; Blankenship, R.; Small, G. J. Energy Transfer and Spectral Dynamics of the Three Lowest Energy Q_y-States of the Fenna-Matthews-Olson Antenna Complex. *J. Phys. Chem. B* **1999**, *103*, 5736−5741.

(33) Wu, H.-M.; Rätsep, M.; Lee, I.-J.; Cogdell, R. J.; Small, G. J. Exciton Level Structure and Energy Disorder of the B850 Ring of the LH2 Antenna Complex. *J. Phys. Chem. B* **1997**, *101*, 7654−7663.

(34) den Hartog, F. T. H.; van Papendrecht, C.; Störkel, U.; Völker, S. Protein Dynamics in Photosystem II Complexes of Green Plants Studied by Time-Resolved Hole-Burning. *J. Phys. Chem. B* **1999**, *103*, 1375−1380.

(35) Reinot, T.; Dang, N. C.; Small, G. J. A Model for Persistent Hole Burned Spectra and Hole Growth Kinetics that Includes Photoproduct Absorption: Application to Free Base Phthalocyanine in Hyperquenched Glassy Ortho-dichlorobenzene at 5 K. *J. Chem. Phys.* **2003**, *119*, 10404−10414.

(36) Reinot, T.; Small, G. J. Modeling of Dispersive Non-photochemical Hole Growth Kinetics Data. Al-phthalocyanine Tetrasulphonate in Hyperquenched Glassy Water. *J. Chem. Phys.* **2000**, *113*, 10207−10214.

(37) Reinot, T.; Hayes, J. M.; Small, G. J. Laser-induced Hole Filling and Spectral Diffusion of Aluminum Phthalocyanine Tetrasulfonate in Hyperquenched Glassy Films. *J. Chem. Phys.* **1999**, *110*, 4820−4827.

(38) Oikawa, H.; Fujiyoshi, S.; Dewa, T.; Nango, M.; Matsushita, M. How Deep is the Potential Well Confining a Protein in a Specific Conformation? A Single-molecule Study on Temperature Dependence of Conformational Change between 5 and 18 K. *J. Am. Chem. Soc.* **2008**, *130*, 4580−4581.

(39) Love, S. P.; Mungan, C. E.; Sievers, A. J.; Campbell, J. A. Persistent Infrared Spectral Hole Burning of Tb^{3+} in the Glasslike Mixed Crystal $Ba_{1-x-y}La_xTb_yF_{2+x+y}$. *J. Opt. Soc. Am. B* **1992**, *9*, 794−799.

(40) Baier, J.; Richter, M. F.; Cogdell, R. J.; Oellerich, S.; Köhler, J. Determination of the Spectral Diffusion Kernel of a Protein by Single-Molecule Spectroscopy. *Phys. Rev. Lett.* **2008**, *100*, 018108-1−018108-4.

(41) Köhler, W.; Friedrich, J. Probing of Conformational Relaxation Processes of Proteins by Frequency Labeling of Opical States. *J. Chem. Phys.* **1989**, *90*, 1270−1273.

(42) Shu, L.; Small, G. J. On the Mechanism of Nonphotochemical Hole Burning of Optical Transitions in Amorphous Solids. *Chem. Phys.* **1990**, *141*, 447−455.

(43) Najafi, M.; Zazubovich, V. Monte-Carlo Modeling of Spectral Diffusion Employing Multi-well Protein Energy Landscapes: Applica-

tion to Pigment-Protein Complexes Involved in Photosynthesis. *J. Phys. Chem. B* **2015**, submitted.

(44) Kiyanagi, R.; Kimura, H.; Watanabe, M.; Noda, Y.; Mochida, T.; Sugawara, T. Indication of Tunneling State of Hydrogen Atom in Hydrogen-Bonded Material 5-Bromo-9-hydroxyphenalenon Studied by X-ray and Neutron Diffractions. *J. Phys. Soc. Jpn.* **2008**, *77*, 064602-1−064602-7.

(45) Hamilton, W. C. *Hydrogen Bonding in Solids*; Benjamin: New York, Amsterdam, 1968.

(46) Frauenfelder, H.; Petsko, G. A.; Tsernoglou, D. Temperature-dependent X-ray Diffraction as a Probe of Protein Structural Dynamics. *Nature* **1979**, *280*, 558−563.

(47) Huber, R. Flexibility and Rigidity of Proteins and Protein-Pigment Complexes. *Angew. Chem.* **1988**, *100*, 79−88.

(48) Zollfrank, J.; Friedrich, J. Spectral Holes under Pressure: Proteins and Glasses. *J. Opt. Soc. Am. B* **1992**, *9*, 956−961.

(49) Brecht, M.; Studier, H.; Radics, V.; Nieder, J. B.; Bittl, R. Spectral Diffusion Induced by Proton Dynamics in Pigment-Protein Complexes. *J. Am. Chem. Soc.* **2008**, *130*, 17487−17493.

(50) Fritsch, K.; Friedrich, J.; Parak, F.; Skinner, J. L. Spectral Diffusion and the Energy Landscape of a Protein. *Proc. Natl. Acad. Sci. U.S.A.* **1996**, *93*, 15141−15145.

(51) Brecht, M.; Radics, V.; Nieder, J. B.; Bittl, R. Protein Dynamics-induced Variation of Excitation Energy Transfer Pathways. *Proc. Natl. Acad. Sci. U.S.A.* **2009**, *106*, 11857−11861.